Remote Recession Measurements of Wire-Seeded PICA Samples in an Arc-Jet Flow

Michael Winter[1]
University of Kentucky, Department of Mechanical Engineering, Lexington, KY 40506-0503, USA

Bradley D. Butler[2], **Paul M. Danehy**[3], **Scott Splinter**[4]
NASA Langley Research Center, Hampton, VA 23681-2199, USA

Margaret Stackpoole[5]
NASA Ames Research Center, Moffett Field, CA 94035-1000, USA

Various methods for remote recession sensing of PICA have been developed and several seeding methods have been tested. The most recent method involved seeding the ablator with wires fed to the sample from the backside with a defined amount of PICA left towards the upstream front of the sample. This seed method mimics the installation of in-depth thermocouples as they are frequently used in ground testing and flight. Arc-jet tests were conducted in the NASA Langley HYMETS facility at a heat flux of 320 W/cm^2. The emission of the post-shock layer was observed in spectral resolution from the side along an optical axis perpendicular to the arc-jet flow and from the front, looking at the sample surface from an upstream position. Various metallic seed materials with different melting points were used. In addition to the emission spectroscopy measurements, the samples were monitored during the tests through pyrometry and videography. The time resolved response of the seeded material is described and compared to earlier tests with different seeding methods. The combination of seed materials was found to be critical for the selection of emission signatures characteristic for the material recession which can be isolated in the final emission spectra.

I. Introduction and Motivation

THE development of materials for reliable thermal protection systems (TPS) for atmospheric entries requires extensive material testing in ground test facilities under conditions relevant to high speed re-entry such as the NASA Ames arc-jets. However, even these high power facilities are not capable of reproducing real flight conditions.[1] Instead, an extrapolation of the ground test data to atmospheric entry conditions is necessary. This is achieved through aerothermochemistry simulation codes. Thus, aerothermochemistry and material response simulations have become very important tool for designing new TPS systems. Material recession and charring are two major processes determining the performance of ablative heat shield materials. For validation of aerothermochemistry and material response codes, time-accurate knowledge of recession and char depth is considered valuable information, especially during flight.

Electro-mechanical recession sensors have been developed[2] but require substantial on-board instrumentation adding mass and complexity. In the recent work, a methodology for recession measurements through the detection of seed elements buried at known depths inside the TPS material was developed.[3,4,5] The basic idea of remote recession sensing is to seed specific materials at a known depths inside the ablative material. Once recession reaches

[1] Assistant Professor, Department of Mechanical Engineering, 151 Ralph G. Anderson Building, Lexington KY 40506-053, USA, Associate Fellow AIAA.
[2] Student Intern NASA Langley, Student Member AIAA.
[3] Research Scientist, Advanced Measurements and Data Systems Branch, MS 493. Associate Fellow AIAA.
[4] Aerospace Engineer, Structural Mechanics and Concepts Branch, M/S 190, AIAA Member.
[5] Senior Research Scientist, Thermal Protection Materials and Systems Branch, NASA Ames Research Center,

the seeding depth, the seed material comes in contact with the plasma, is gasified, and transported into the hot region of the post-shock layer by diffusion processes where the characteristic emission signatures can be detected by emission spectroscopy. Detection could be accomplished through ground based or airborne observation as performed during the Stardust[6] and Hayabusa[6] re-entries, through on-board spectrometers, or even through formation flight. A feasibility study in a NASA Ames arc-jet facility was successfully conducted and showed promising results.[3] Seeding PICA samples though insertion of epoxy disks which contain the seed materials or through PICA plugs where the seed materials were introduced during the curing process has been demonstrated in arc-jet testing in the HYMETS facility at NASA Langley.[4,5]

The most recent tests conclude the assessment of different seeding methods by investigating seeding of PICA through metal wires, mounted in the heat shield material like thermocouples. The advantage of this method is that the application of in-depth thermocouples is already flight qualified and accepted from a system engineering point of view. In this paper, the application of metal seed wires is demonstrated during arc-jet tests.

II. Experimental Setups for HYMETS Testing

The NASA Langley HYMETS arc-jet is one of the NASA ground test facilities for the experimental investigation of thermal protection materials. A 400 kW power supply is used to run a segmented-constrictor direct-current electric arc heater, which serves as the arc plasma generator. Test gasses are injected tangentially into the bore to produce a vortex flow, which spin-stabilizes the electric arc of the plasma generator. The heated mixture is then accelerated through a convergent-divergent 8-degree half-angle Mach 5 conical nozzle with a 12.7-mm diameter throat. To increase the footprint of the arc and thus protect the electrodes from rapid oxidation, argon (Ar) is injected near the anode. After passing through the test section, the flow exhausts into a 0.6-m diameter by 0.9-m long vacuum test chamber. A high capacity pumping system is used to evacuate the stagnated flow from the facility after being cooled. Depending on the tunnel conditions, the facility can be operated by a single technician, continuously, and for several hours.[8,9]

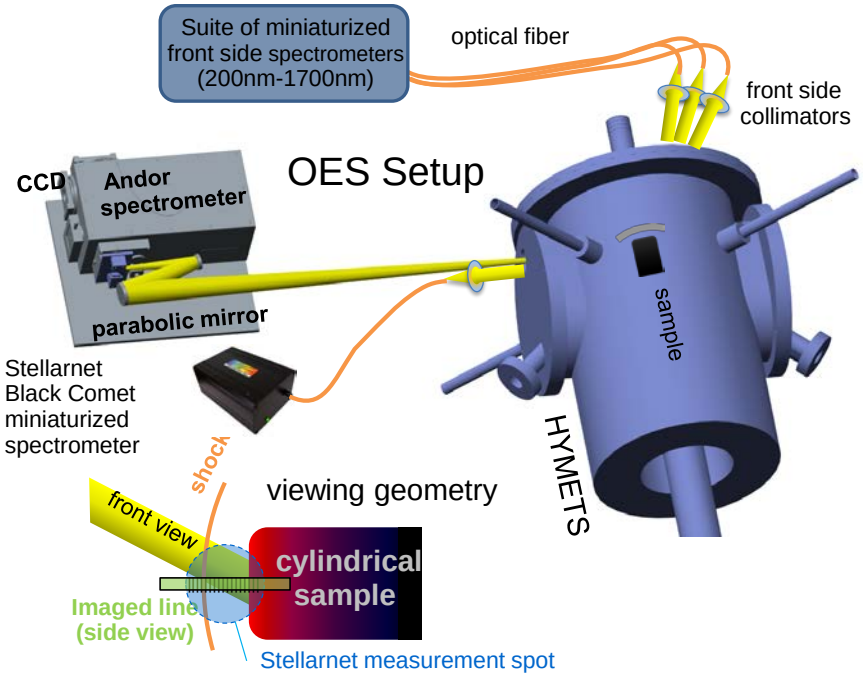

Figure 1. Setup for optical emission spectroscopy (OES) from the side with an Andor imaging spectrometer and a miniaturized fiber coupled spectrometer, the suite of miniaturized fiber coupled spectrometers viewing the specimen stagnation surface, and associated viewing geometries inside HYMETS.

For the emission spectroscopy measurements, an Andor Shamrock spectrometer with 500 mm focal length in combination with a Princeton Instruments PIXIS:400BR_eXcelon CCD was used for spectral dispersion and detection. The spectrometer observed the stagnation region in front of the PICA samples through a side window of the HYMETS facility. The 150 lines/mm grating allowed for simultaneous detection of a wavelength range from 204 nm to 550 nm with a spectral resolution of ~0.26 nm. A 445 mm focal length parabolic mirror and several

redirecting mirrors were used to image a horizontal line onto the vertical entrance slit of the spectrometer. Since the sample position was not directly accessible through the side window, an additional periscope consisting of two parallel mirrors was placed inside the vacuum chamber to give a perpendicular line of sight onto the flow axis. In addition, several fiber-fed miniaturized spectrometers were pointed at the post-shock region. A Thorlabs mirror collimator was used to image the entire post shock region including part of the sample side in form of a circular spot with 20 mm diameter onto an optical fiber feeding a Stellarnet Black Comet miniaturized spectrometer with a spectral range from 200 nm to 1,100 nm and a pixel resolution between 0.54 nm at 200 nm and 0.35 nm at 1,000 nm to provide overview spectroscopy from the side. A suite of three spectrometers (OceanOptics USB 4000, 350 nm to 1050 nm, OceanOptics NIRQuest 512, 900 nm to 1700 nm, and a Thorlabs CCS150 UV, 200 nm to 400 nm) were pointed at the sample front surface providing emission spectra from 200 nm to 1700nm. Time-resolved spectra were taken over the insertion time of the sample. Figure 1 illustrates the emission spectroscopy setups and the viewing geometry inside the HYMETS chamber.

The CCD array height of 8 mm of the Pixis camera allowed for monitoring a line of 22 mm length inside the HYMETS facility. Focusing was done by imaging the sample at the measurement position on the spectrometer camera with the grating tuned to zero order therefore producing an image without spectral dispersion. Intensity calibration of both spectrometers was done through measuring the emission of a miniaturized spectral radiance source (Gigahertz-Optik BN-0102) calibrated between 300 nm and 1,100 nm and a deuterium lamp (Bentham CL3) calibrated to spectral irradiance between 200 nm and 400 nm. The irradiance values from the Deuterium lamp were used to obtain the spectral sensitivity in the UV and were scaled to the radiance values obtained from the Gigahertz-Optik lamp in the overlapping spectral region to achieve a calibration to spectral radiance over the entire measured spectrum.

III. Experimental Data and Preliminary Analysis

Five samples were prepared with seed wires of 1 mm diameter (0.04 inches) made from W, Ti, Al, In, V, and Ag. These metals were selected because they provide low electronic excitation energies to guarantee strong emission lines even at lower temperatures in the boundary layer close to the surface. They cover a wide range of melting temperatures which was found to be an important parameter in earlier measurements. Seed materials with melting temperatures lower than the surface temperature were found to show up in the emission spectra before the recession reaches the actual seeding depth. In addition, in-depth Type-K thermocouples (TCs) were installed in the samples, adding the emission of Mn, Cr, and Ni to the seed materials, once the operational temperature of 1,500 K was exceeded at the in-depth position the thermocouple and its melting temperature was reached. As a baseline, the seed wires were oriented in axial direction perpendicular to the sample front surface. However, one alternate seeding geometry with wires oriented in radial direction parallel to the front surface was tested, too. Testing was performed at a nominal cold wall heat flux of 320 W/m^2 and a stagnation pressure of 23 Torr. Table 1 summarizes the investigated configurations, the seed materials and depths (measured from x-ray images where available, the nominal design depth for the first two samples), and the integral and average recession, Table 2 lists the melting points of the elements used.

Table 1. Seeding information for the wire seeded samples.

Sample	*Seeding method*	*Seed elements*	*Seeding Depth, mm*	*Insertion Duration*	*Recession*	*Recession Rate, mm/s*
PICA-A	axial wires	W, In, TC (Mn, Cr, Ni)	1.65 (nominal)	30.6 s	3.3 mm	0.107
PICA-B	axial wires	Ag, V, TC (Mn, Cr, Ni)	1.65 (nominal)	31 s	3.1 mm	0.099
PICA-C	axial wires	Ti, Al, TC1 TC2 (Mn, Cr, Ni)	1.65 11.8	31.1 s	3.0 mm	0.097
PICA-D	axial wires	Ti, Al, In, TC	1.73, 2.52 9,98, 12.25	30.4 s	3.3 mm	0.107
PICA-Z	radial wires	V, Ag, Al	0.6,2.0,3.4,	41.1 s	3.5 mm	0.088

Table 2. Melting temperatures of the selected seeding materials and thermocouple metal.

Titanium (Ti)	*Vanadium (V)*	*Indium (In)*	*Aluminum (Al)*	*Silver (Ag)*	*Tungsten (W)*	*TC (Mn, Cr, Ni)*
1941 K	2183 K	430 K	933 K	1235 K	3695 K	1673

The high-resolution emission spectroscopy data acquired from the side view with the Andor spectrometer was taken with an entrance slit width of 30 μm, and an acquisition time of 20 ms at a frame rate of about 3 frames per second. In each frame the post-shock region from the shock to the sample surface (which is about 3 mm) is spatially resolved showing the distribution of the observed radiation along the stagnation line. However, for the analysis of the seed elements, the temporal change contains the most important information, i.e. when do individual species show up in the measured spectra. Therefore, the spatial information in the spectra was ignored by summing up the first 100 spectra upstream of the sample surface in each frame after being individually calibrated, showing the total spectral emission of the entire post shock layer. The resulting spectra were plotted versus time after sample insertion as shown in Figs. 2 to 6, along with predicted emission of the seed elements calculated based on NIST data of the electronically excited states under the assumption of a Boltzmann distribution at 6,000 K. The chosen temperature was considered uncritical, since the main interest in this case lies in the wavelength position of the different lines and not in their intensity. The strongest emission in the measured spectra comes from CN molecular bands with the strongest band around 388 nm. In addition atom lines from the seed elements and from Mn, Ni, and Cr from the in-depth thermocouple were monitored.

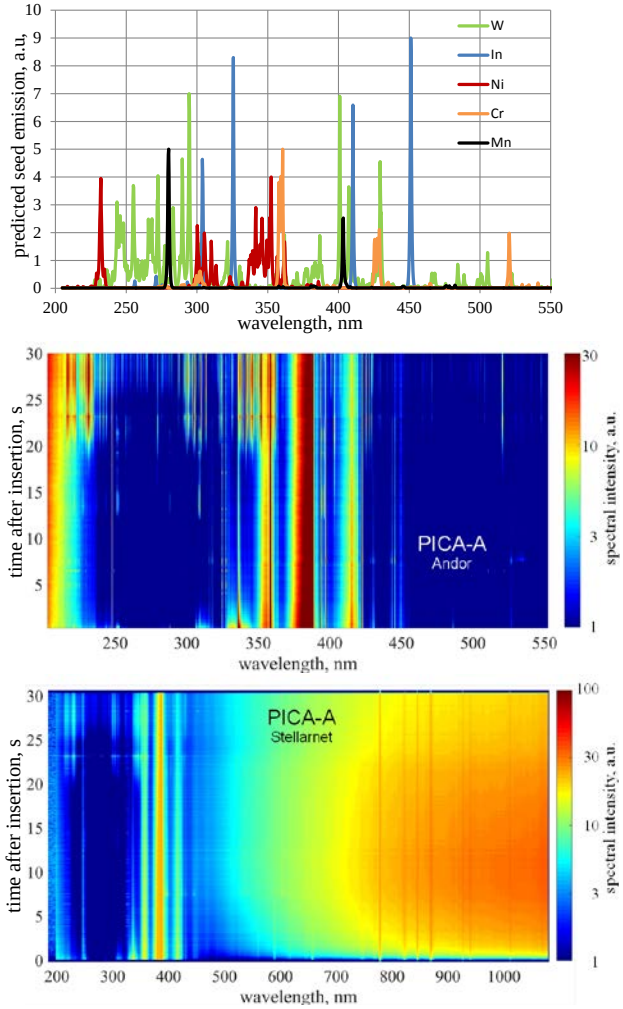

Figure 2. Predicted seed element emission and time trace of the spectral emission of the entire post-shock layer from the side view during the insertion of PICA-A, seeded with co-axial In and W wires and instrumented with two in-depth thermocouples.

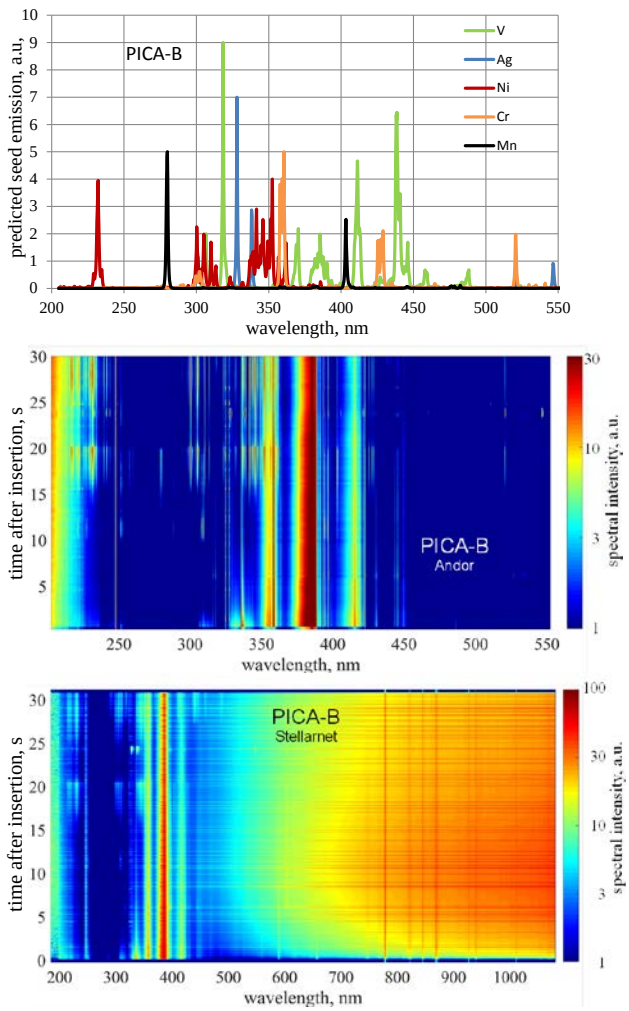

Figure 3. Predicted seed element emission and time trace of the spectral emission of the entire post-shock layer from the side view (Andor left, Stellarnet right) during the insertion of PICA-B, seeded with co-axial Ag and V wires and instrumented with two in-depth thermocouples.

For the fiber-fed Stellarnet Black comet, a measurement spot diameter of 20 mm diameter at the sample position was obtained with the Thorlabs mirror collimator, partly covering the sample surface, as shown schematically in

Fig. 1, and therefore showing significant thermal continuum emission from the glowing surface. Spectra were taken with exposure times of 5 ms for the PICA-A sample and 2 ms for the other samples. In the data analysis method it became clear that this reduction in exposure time caused random oscillations in the spectrometer response which was verified by measuring a continuous lamp with different exposure times. Therefore, the oscillations, seen as horizontal lines in the Stellanet signals in Figs. 3 to 5, which are not seen in the Andor signals, are not due to plasma oscillations. The oscillations seen with the PICA-Z sample in Fig. 6 at times greater than 20 s after sample insertion, however, are real and assigned to molten metal on the surface from the wires oriented parallel to the sample surface. The sampling rate of the Stellarnet spectrometer was reduced from about 25 Hz for the samples A, B, and C to about 3 Hz for the last two samples D and Z. For the last three samples C, D, and Z, x-ray pictures of the samples before being tested were available which illustrate the wire and thermocouple positions inside the PICA material. The data presented here focus on the side view spectra, data from the front view spectrometers is still being analyzed. Figures 2 to 6 show the time traces obtained from the two side view spectrometers and x-ray pictures of the samples before testing where available.

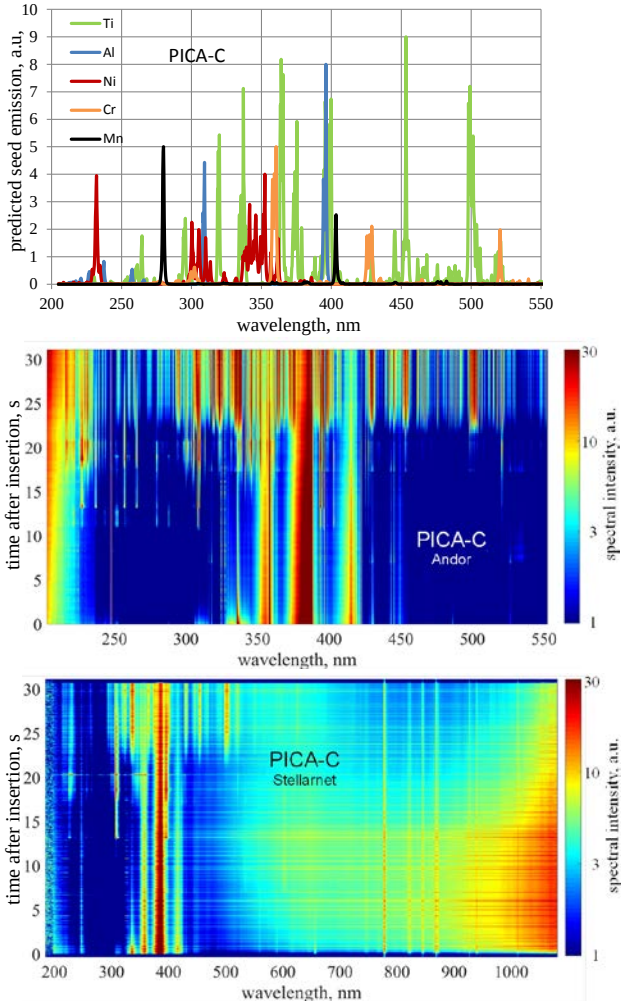

Figure 4. Predicted seed element emission and time trace of the spectral emission of the entire post-shock layer from the side view during the insertion of PICA-C, seeded with co-axial Al and Ti wires and instrumented with two in-depth thermocouples.

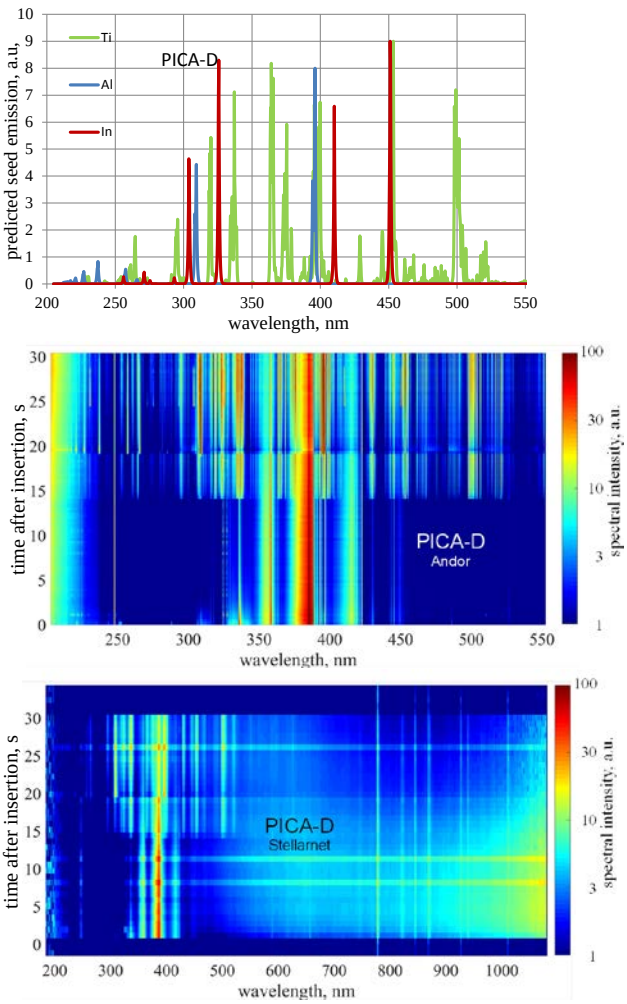

Figure 5. Predicted seed element emission and time trace of the spectral emission of the entire post-shock layer from the side view during the insertion of PICA-D, seeded with co-axial Al, Ti, and In wires and instrumented with one in-depth thermocouple.

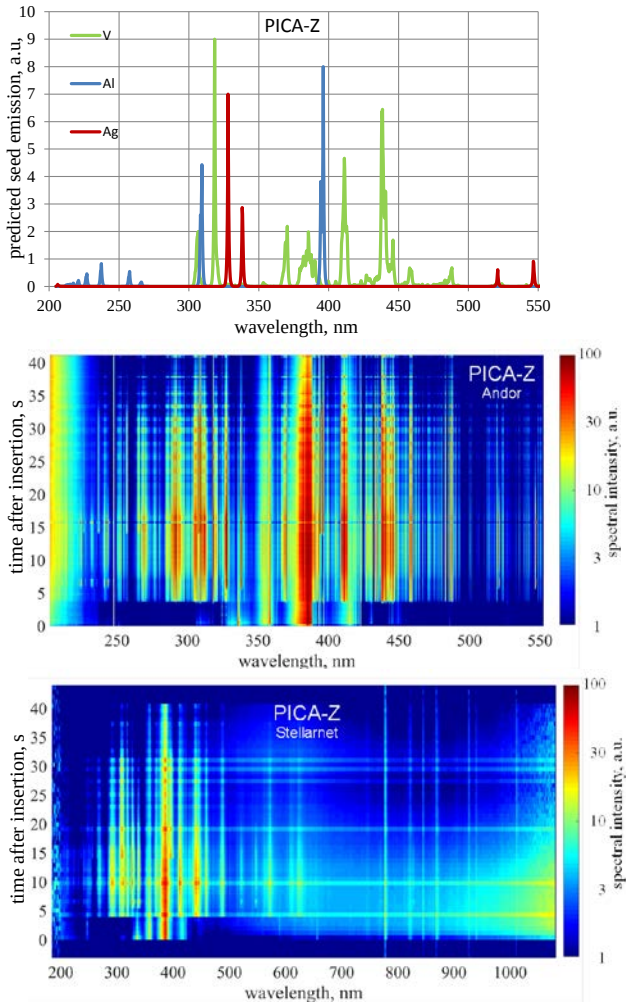

Figure 6. Predicted seed element emission and time trace of the spectral emission of the entire post-shock layer from the side view during the insertion of PICA-Z, seeded with V, Ag, and Al wires oriented parallel to the sample surface.

For a more detailed analysis, line integrals were extracted from the spectra by integrating the line emission and subtracting a trapezoidal background based on the corner values of the integration borders to account for underlying continuum emission from the glowing sample or interfering emission from other plasma species. If the emission line of concern is not present, though, this integration can generate negative values as it is the case for the tungsten line integral in Fig. 7 (b). If multiple emission lines were available, the shown emission for each element is the average of the lines which could be separated from the plasma background. These line integrals were normalized to illustrate the time history of the emission of each element. The surface temperatures of each sample measured with a facility pyrometer and, where available, in-depth temperature traces are shown. Except for sample PICA-A, the sample surface was monitored through color videos of the sample insertion. From these videos, images were extracted at times when changes on the surface became visible, i.e., when the recession reached the seeding depth at a seed element location to be compared with the spectral response. Where available, x-ray images of the samples before testing are added. In general, the signals from both spectrometers agreed well with each other unless the lower spectral resolution of the Stellarnet spectrometer did not allow for a clear separation of the emission line of concern from the plasma background which happened for the In line during testing of sample PICA-A.

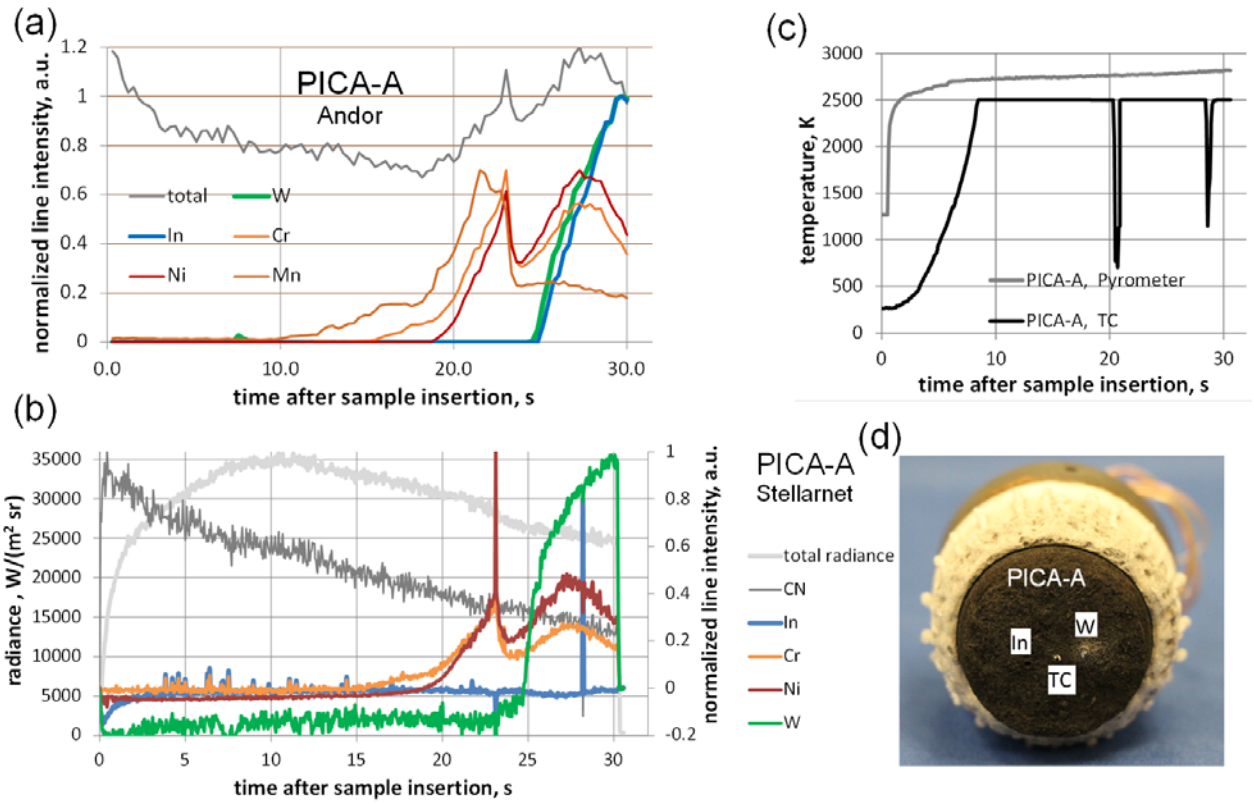

Figure 7. Recession analysis of sample PICA-A, seeded with co-axial In and W wires and instrumented with two in-depth thermocouples: (a) normalized line integrals extracted from the Andor spectra vs. time after sample insertion; (b) normalized line integrals extracted from the Stellarnet spectra vs. time after sample insertion; (c) surface temperature from pyrometer measurements and in-depth thermocouple response vs. time after sample insertion, and (d) post-test picture of the sample.

In the Andor data for PICA-A, at about 13 s after sample insertion first signals of Mn become visible, followed by first emission of Cr at 15 s and of Ni at about 18 s. All these line integrals increase up to a peak value at about 23 s, then decrease again and show a second local maximum at 27 s, and remain visible until the end of the test. A very similar trend is observed in the Stellarnet data, although no reasonable Mn signal could be separated from the plasma background due to the lower spectral resolution. The peak values, however, are sharper in the Stellarnet spectra. The emission of W becomes visible at about 25 s into the test with both spectrometer and peaks at the end of the test. The line integrals of In show a very similar trend in the Andor data, but result in a sharp peak at about 28 s with the Stellarnet spectrometer. The seed wires and the thermocouple have a nominal distance of 1.65 mm to the sample surface. With the an average recession rate of 0.107 mm/s obtained from thickness measurements before and after the test, the seeding depth should have been reached after 16.4 s which is much earlier than the 25 s at which significant line emission from seed elements appears in the spectra. A probable explanation seems to be inadequate assembly of the samples with the seed wires, which were inserted from the back of the sample, were not reaching far enough into the sample material. In the post-test image, it can be seen that the tungsten wire extends from the surface and therefore showed a slower recession rate than the PICA material. Mn emission, on the other hand, is already seen at 10 s in the Andor spectra, followed by Cr at 15 s, and Ni at 18.5 s. The corresponding values from the Stellarnet spectra are shifted towards later times, All TC line integrals increase with test time, show a sharp peak at 23 s, and a second local maximum at about 27.5 s in the data of both spectrometers. As will be shown later in the data of other the samples PICA-B and PICA-C, the sharp peak usually correlates with the appearance of the thermocouple wire in the video, meaning at this sharp peak, recession reaches the TC wire. The emission of Mn, Cr, and Ni before recession reaches the wire is explained is explained by the metal melting inside the PICA body once the in-depth temperature gets sufficiently high and molten metal diffusing through the porous PICA most probably through capillary effects.

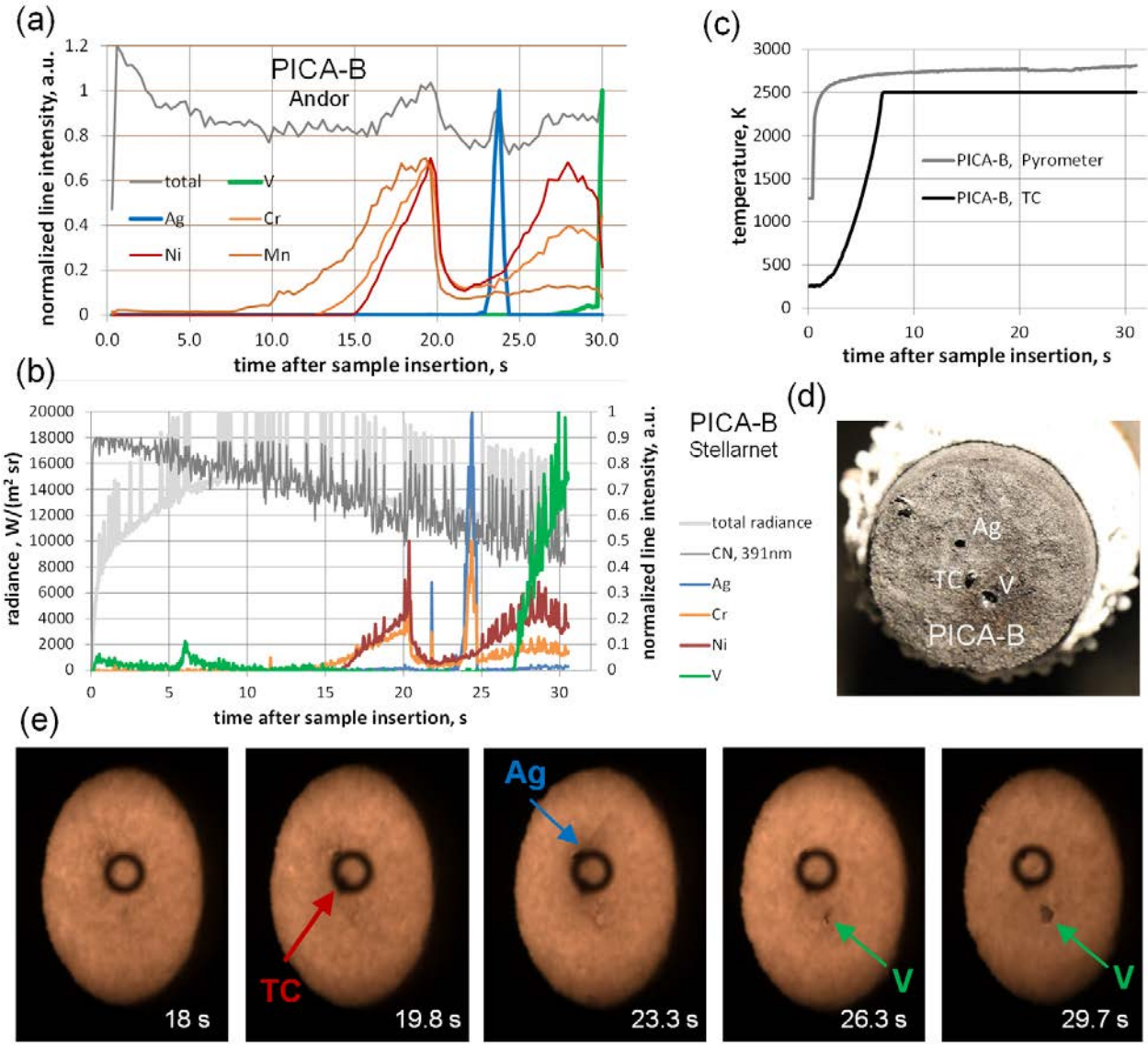

Figure 8. Recession analysis of sample PICA-B, seeded with co-axial Ag and V wires and instrumented with two in-depth thermocouples: (a) normalized line integrals extracted from the Andor spectra vs. time after sample insertion, (b) normalized line integrals extracted from the Stellarnet spectra vs. time after sample insertion, (c) surface temperature from pyrometer measurements and in-depth thermocouple response vs. time after sample insertion, (d) post-test picture of the sample, and (e) surface images at characteristic times after sample insertion.

With the PICA-B sample, a very similar trend is seen for the TC elements. Again, Mn shows up first (at about 7.5 s) followed by Cr and Ni at 13 s and 15 s, respectively. The emission of these elements peaks shortly before 20 s, drops down, and shows a second maximum at about 27 s. A comparison with the video data shows a dark spot at the location of the thermocouple appearing at 19.8 s which corresponds well to the first maximum in TC element emission. (The black circle in the video images is no flow pattern but a marker in the optics indicating where the pyrometer is measuring.) Ag emission shows up as a sharp peak in both spectrometers at about 23 s, which again corresponds well to the video data where a first indication of recession reaching the seeding depth of Ag is seen at 23.3 s. In the video data, the V wire becomes first visible at 26.3 s, vanadium emission starts showing up in both spectra at about the same time. Again, from analysis of both the video and spectrometer data, which agree very well, the actual distance of the seed wires to the surface seems to exceed the nominal seed depth of 1.65 mm which would indicate recession should reach the seed wires around 17 s. From a comparison of video and spectral data, it is concluded that the first maximum of the TC element emission indicates recession reaching the thermocouple

location. The discrepancy between the nominal seed depth of the wires and the observations acquired in the facility led to the use of x-ray imagery to determine the actual location of the wires prior to the subsequent tests.

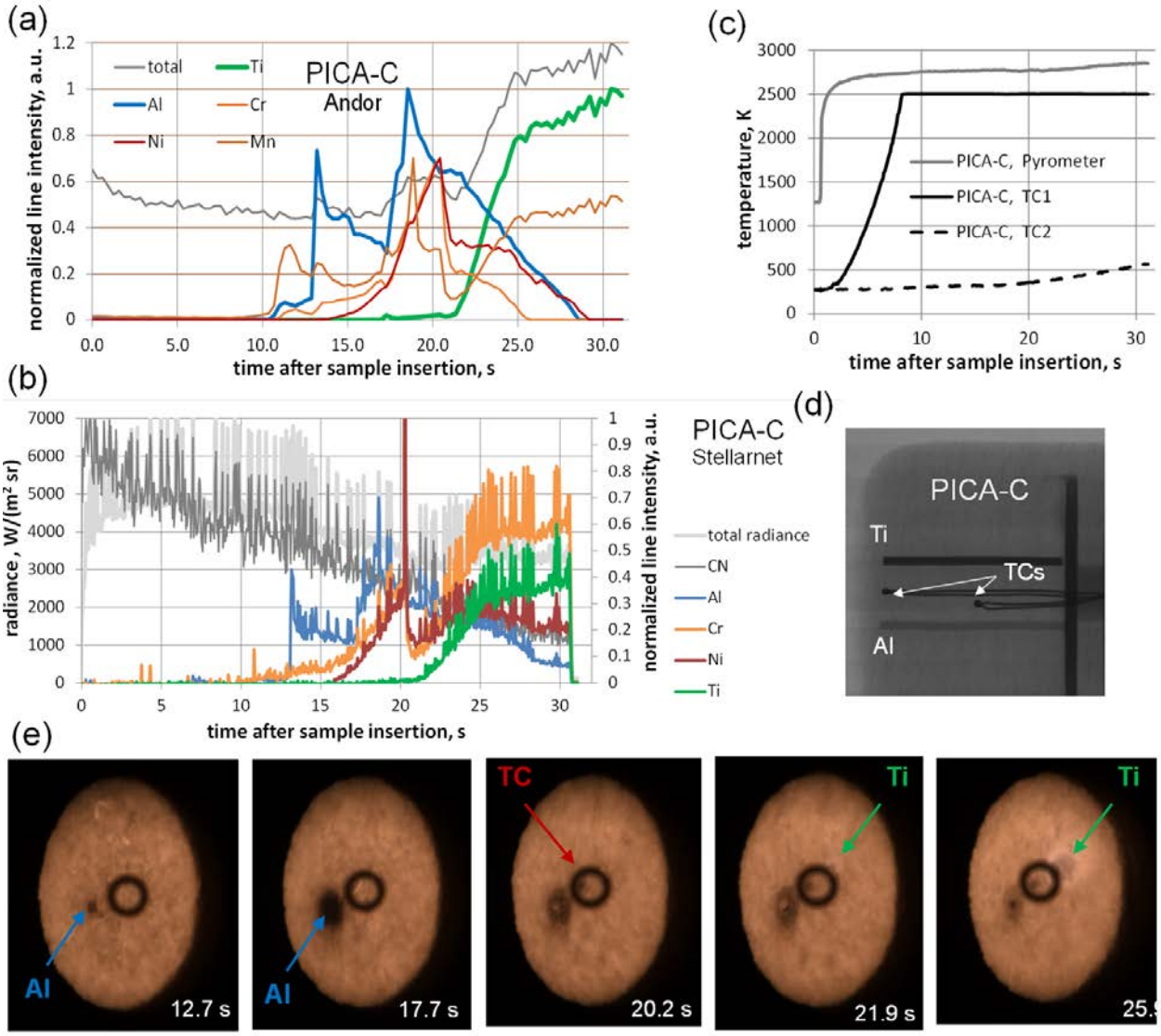

Figure 9. Recession analysis of sample PICA-C, seeded with co-axial Al and Ti wires and instrumented with two in-depth thermocouples: (a) normalized line integrals extracted from the Andor spectra vs. time after sample insertion; (b) normalized line integrals extracted from the Stellarnet spectra vs. time after sample insertion; (c) surface temperature from pyrometer measurements and in-depth thermocouple response vs. time after sample insertion, (d) x-ray image of the sample before testing, and (e) surface images at characteristic times after sample insertion.

For the PICA-C sample, an x-ray image of the sample before testing is available, showing the Al and Ti seed wires and the thermocouple at distances to the sample surface of 1.85 mm, 2.25 mm, and 2.05 mm, respectively. The spectroscopic data shows Mn emission becoming visible at about 10 s into the test, quickly followed by Cr and Al. The Al wire becomes visible in the test video at 12.7 s which correspond well to a strong increase of the Al emission in the Andor spectra and to the first appearance of Al emission in the Stellarnet data. The video indicates the aluminum spreading out at the surface with a maximum spot size around 18 s which corresponds to the maximum of Al emission with both spectrometers. From the average recession rate, the seeding depth should be reached by recession after 19 s. This phenomenon of Al emission showing up before recession reaches the seeding depth has been already observed in earlier tests,[4] and is similar to the TC emission for ICA-A explained by Al melting inside

the PICA body and diffusing through the porous PICA most probably through capillary effects. As already hypothesized in the analysis of the PICA-A results, the same effects seem to occur with the thermocouple elements. The thermocouple wire becomes visible in the test video at 20 s which, again is the time the TC element emissions peak but emission of Mn, Cr, and Ni is visible clearly before that time. The Ti wire appears in the video at 22 s which is when the Ti emission starts to become visible with both spectrometers. The times in which the different elements become visible in the video agree within ~1 s with the times calculated from the seeding depth from the x-ray picture using the average recession rate from pre- and post-test thickness measurements.

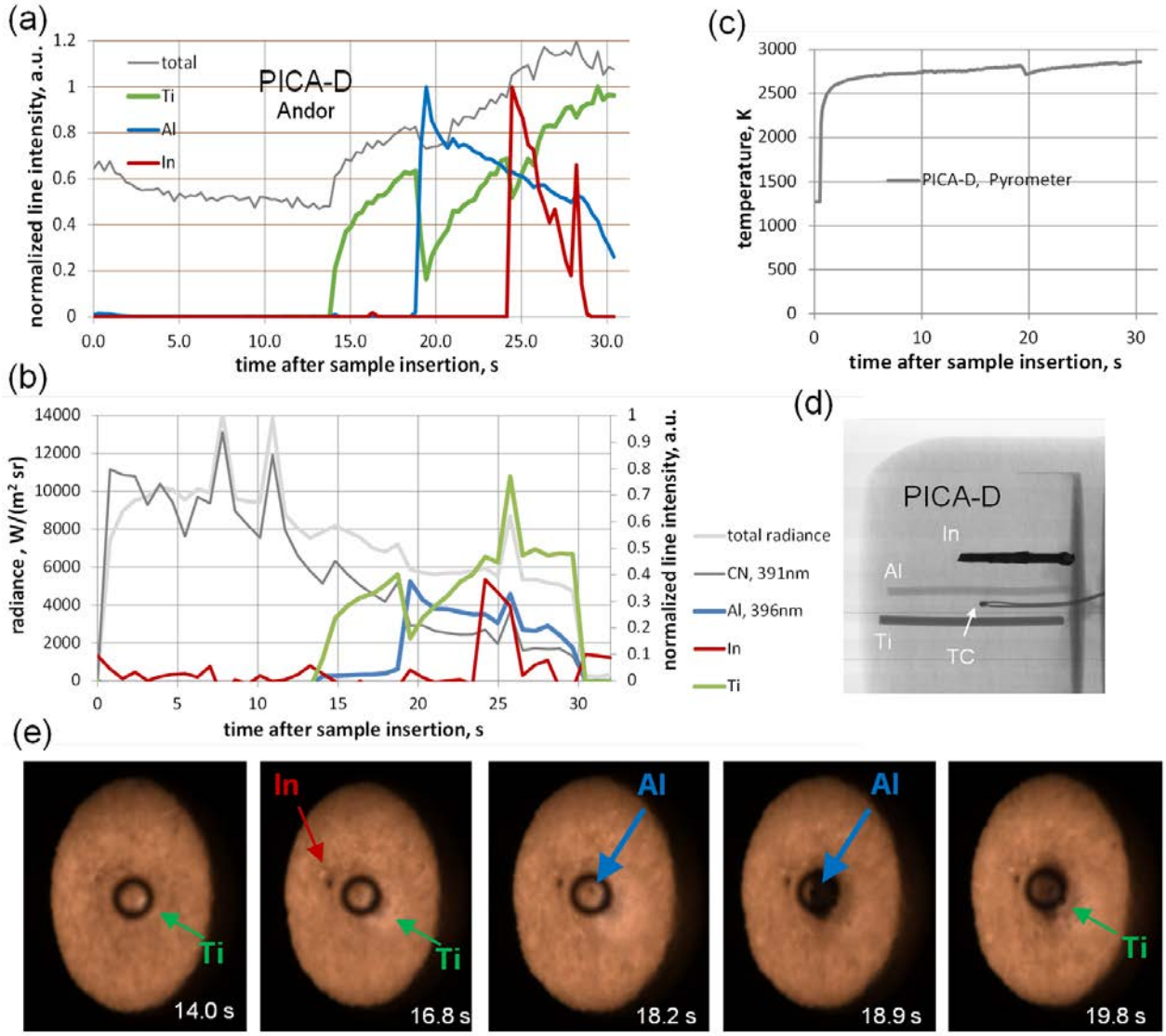

Figure 10. Recession analysis of sample PICA-D, seeded with co-axial Ti, Al, and In wires and instrumented with one in-depth thermocouple: (a) normalized line integrals extracted from the Andor spectra vs. time after sample insertion; (b) normalized line integrals extracted from the Stellarnet spectra vs. time after sample insertion; (c) surface temperature from pyrometer measurements and in-depth thermocouple response vs. time after sample insertion, (d) x-ray image of the sample before testing, and (e) surface images at characteristic times after sample insertion.

For the PICA-D sample, distances of the seed wires to the sample surface were estimated from the pre-test x-ray image to be 1.73 mm for Ti, 2.52 mm for Al, and 9.98 mm for In. In the video, a first indication of the Ti wire becoming visible is seen at 14 s which is when Ti emission becomes visible with both spectrometers. This time corresponding roughly to the predicted time of 16.3 s, if the average recession rate is used. Although consistent between video and spectral signals, the predicted time for Al to show would be after 24 s using the average recession

rate. A surface change at the Al wire position becomes visible at 18 s, a steep increase in Al emission, however, is seen around 18.5 s. Again, this is assigned to molten aluminum diffusing through the porous PICA to get in touch with the plasma before the seeding depth is reached. The cavity drilled for inserting the In wire extends to a distance of 1.65 mm from the surface, however due to the malleability of the In wire a cavity is formed inside the PICA material. This cavity appears in the video at 16.8 s, however, the In emission does not start before 24 s into the test.

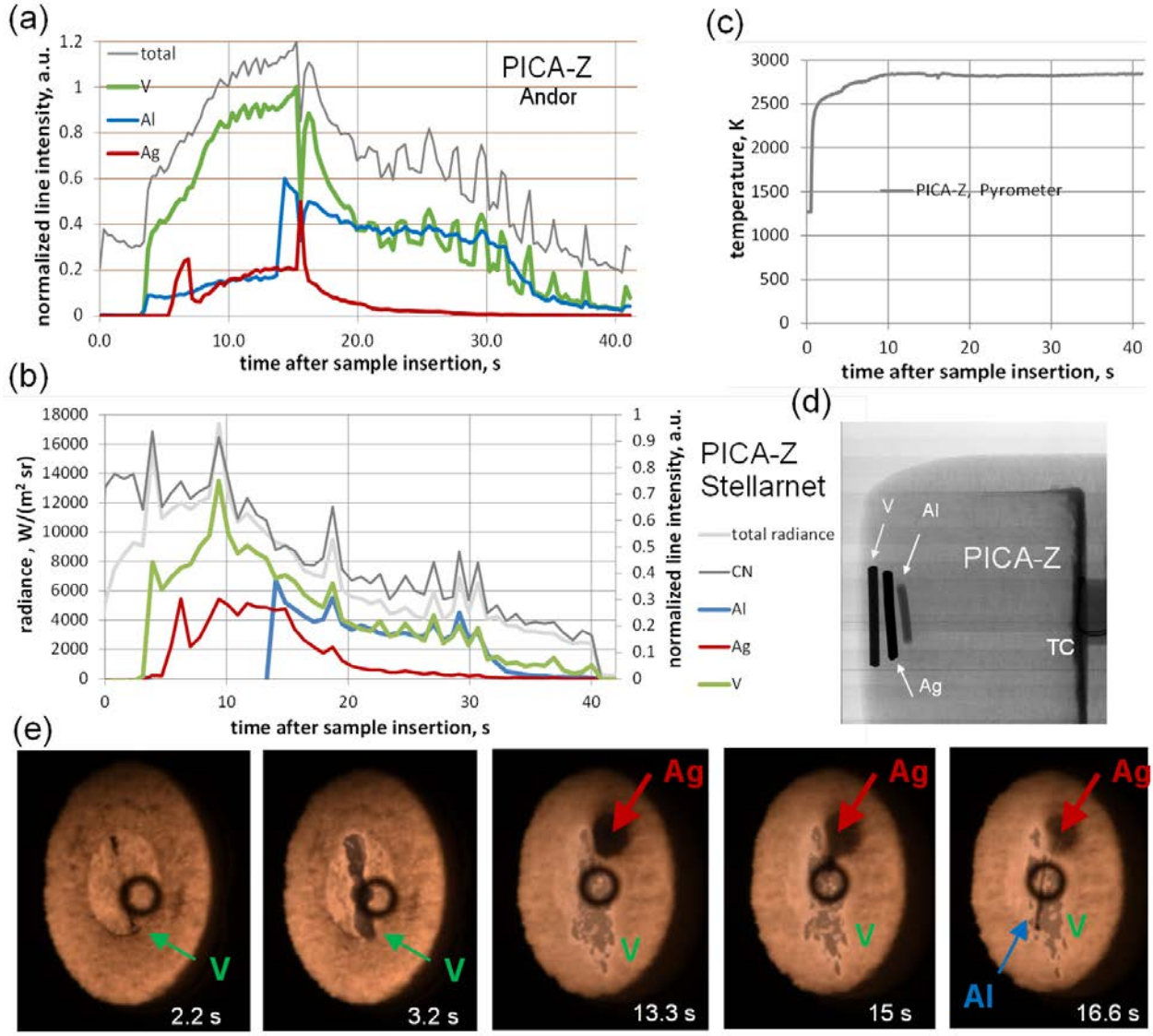

Figure 11. Recession analysis of sample PICA-Z, seeded with V, Ag, and Al wires oriented parallel to the sample surface: (a) normalized line integrals extracted from the Andor spectra vs. time after sample insertion; (b) normalized line integrals extracted from the Stellarnet spectra vs. time after sample insertion; (c) surface temperature from pyrometer measurements and in-depth thermocouple response vs. time after sample insertion, (d) x-ray image of the sample before testing, and (e) surface images at characteristic times after sample insertion.

For the PICA-Z sample, wires were embedded into the surface in the radial direction at different seeding depths to see how larger seed material amounts affect the measurements. The V, Al, and Ag wires were located at distances to the sample surface of 0.6 mm, 2.0 mm, and 3.4 mm, respectively. At 2.2 s after sample insertion, the V wire became visible and was almost completely exposed to the plasma after 3.2 s. For the remaining test time, molten V spread across the surface and was always present. In both spectrometers, V emission started showing up at 3 s, together with Al emission in the Andor spectra. In the Stellarnet data, Al emission was not seen before 13 s into the test. However, V has a large amount of emission lines and is a good emitter so its emission easily interferes with

other lines, in particular with coarse spectral resolution as given with the Stellarnet spectrometer. A large dark spot was seen in the video at the Ag wire position around 13 s which after 20 s, strong fluctuations are seen in the V spectra which seems to result from molten material moving around on the surface. The Al wire finally appears in the video after 16 s. The emission of Ag and Al occurs clearly before the actual seeding depth is reached by recession which, again, is explained by molten metal diffusing through the porous PICA.

To sum up the results, Fig. 12 shows the differences between the time first changes at the seeding position are visible on the surface in the test video (which is considered the time recession reaches the seeding depth) and the time first seeding emission is visible in the spectrum, the time the seed element emission peaks, and the time predicted from the seeding depth divided by the average recession rate (where available, seeding depths estimated from the x-ray images were used, otherwise this value refers to the nominal design depth of 1.65 mm). No values from the test with sample PICA-A are included in Fig. 12 since no test video was available for that test.

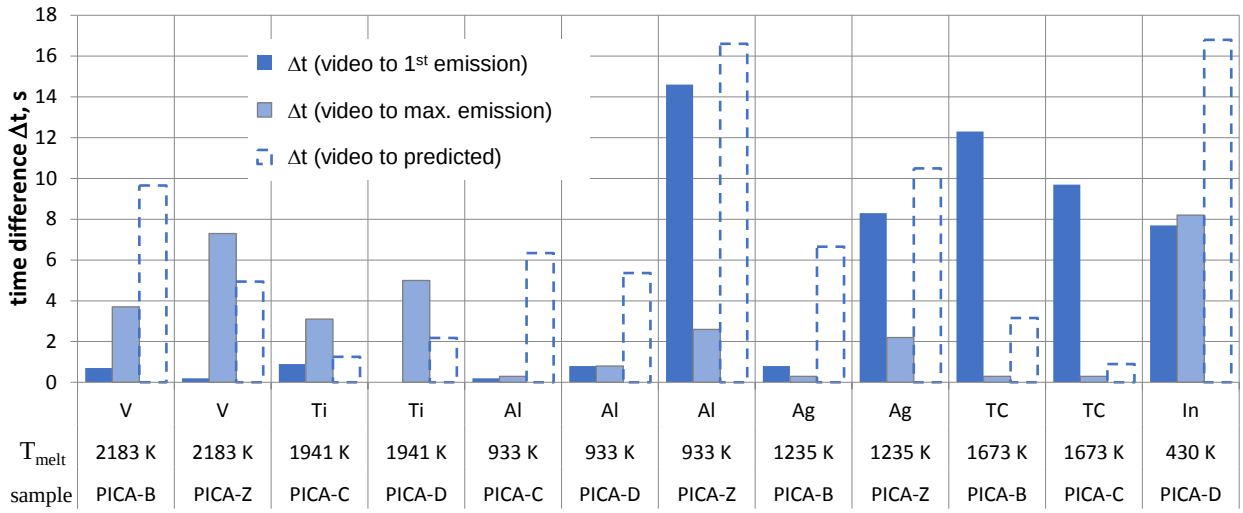

Figure 12. Differences in time between the first sign of surface changes in the test video and first seed element emission showing up in the emission spectra, time of peaking seed element emission, and predicted time the recession reaches the seeding depth, ordered by melting point of each seed element.

For vanadium and titanium, the moment first emission lines show up in the spectrum agrees very well with the first surface changes becoming visible in the test video which means that the seed wire starts emitting as soon as it is exposed to the plasma but not earlier. Surprisingly, that seems to be the case for aluminum as well in the tests with samples PICA-C and D, which is a different behavior from tests with Al embedded in PICA plugs where the Al emission usually showed clearly before the seeding depth was reached.[4] In the test with sample PICA-Z, aluminum shows up early and confirms the anticipated behavior. Also for silver, the results are ambiguous since very small differences between test video and emission spectra were found in the test with sample PICA-B while the PICA-Z results show a bad correlation between video and emission. However, the difference in the results between sample PICA-Z and the other samples might also result from the geometrically different seeding method. In PICA-Z, relatively large amounts of seed metal were embedded close to the surface if compared to the axially mounted wires in the other samples. Inhomogeneous recession over the surface might actually influence the recession behavior. There also might be an effect of the hot vanadium which stayed on the surface over the entire test duration.

The thermocouple emission typically precedes the video data. However, the time of the peak emission correlates well with the time deduced from the test video. In the case of indium, the emission did not correlate with recession. However, indium is very soft which created difficulties in inserting the wire into the hole in the PICA matrix which by itself might be seen as a disqualifying criterion for future applications.

Summary and Conclusions

As the last design configurations in a series of experiments carried out over the past few years to characterize different delivery methods for seed materials into an ablative material for remote recession measurements, metal seed wires of the dimension of thermocouple wires were investigated with PICA material as a carrier. In general, the method of remotely measuring surface recession has been proven, and a successful correlation between recession observed by videos of the sample surfaces and the time spectral emission signatures of the seed elements observed with spectrometers in different wavelength resolution could be established. Seed elements having high melting points worked best. Seed elements with lower melting point showed the tendency to show up in the emission spectra before recession reached the seeding depth. Instead of the first appearance in the measured spectra, a sharp emission peak indicated recession reaching the seeding depth. The emission of aluminum, silver, and thermocouples (Mn, Cr, and Ni) were seen in the measurements clearly before the seeding depth was reached. Once seed materials melt, the liquid material seems to be able to diffuse to the surface, most probably through capillary forces, and get in touch with the plasma, creating emission signatures before the actual seeding depth is reached by recession. The maximum of the emission signatures of the thermocouple elements, however, correlated with recession reaching the thermocouple depth. The time the emission signatures appeared in the post-shock spectra did, however, not always correlate with predicted values if a constant recession rate determined from pre- and post-test material thickness measurements was applied. The best candidates investigated here were tungsten, vanadium, and titanium because their emission correlated best with the recession reaching the seeding depth. Indium proved hard to integrate into the material, at least in wire form. Vanadium showed a good performance but also a large number of emission lines which can have an impact on using various seed elements in the same sample if the V emission overlaps with the emission lines of other seed elements. In comparison to former measurement campaigns, metal seed wires seem a suitable solution if preferred from a system engineering point of view. In terms of performance, seeded PICA plugs seem to be superior to metal wires if only remote recession measurement criteria are considered.

In summary, remote recession measurements of ablative materials were demonstrated as a valuable recession measurement method, in particular for flight applications. The application to a flight mission seems feasible and rather easy to implement if the opportunity of an external observation, as performed in the past for the entries of Stardust and Hayabusa, is given. In general, the design of an onboard measurement system is feasible if a flight spectrometer observing the post-shock region is available. The nature of the seed materials diffusing into the post-shock layer would not require spatial resolution or a direct view onto the surface of such a spectrometer.

Acknowledgments

The work on remote recession measurements and development of facilities and methods for the investigation of gas-surface interactions is supported by NASA Kentucky under NASA awards No: NNX10AL96H and No: NNX13AB12A, and by NASA Ames through the research grant NNX15AN74A. Financial support for the experimental work at NASA Langley was provided by NASA Kentucky EPSCoR Award NNX10AV39A. The authors would like to thank Michael Wright and Nagi Mansour from NASA Ames Research Center, Floyd Taylor and Herb Mefford at the University of Kentucky for their assistance in designing and machining many of the components necessary for this project, Zhaojin Diao and Helmut Koch for their help in preparing the measurement campaign, Gregory Gonzales, Joe Wang, Joel Seibert, and Joe Mach for their support at NASA Ames, along with Jeff Gragg for their support and cooperation during testing at NASA Langley, Wade Jackson for providing the x-ray images, and David Glass for providing travel funds and testing time in the HYMETS facility.

References

[1] Deepak Bose, Kristina Skokova, Michael J. Wright, James Reuther, "Ground-to-Flight Traceability Analysis of Arcjet Testing for the Crew Exploration Vehicle," AIAA 2009-3845, 41st AIAA Thermophysics Conference,22 - 25 June 2009, San Antonio, Texas.

[2] Oishi, T., Martinez, E., "Development and Application of a TPS Ablation Sensor for Flight," *45th AIAA Aerospace Sciences Meeting and Exhibit*, 9-12 January 2008, Reno, NV.

[3] Winter, M. W., Stackpoole, M., Nawaz, A., Gonzales, G. L., Ho, T., "Remote Recession Sensing of Ablative Heat Shield Materials," 52nd AIAA Aerospace Sciences Meeting, 13 - 17 January 2014, National Harbor, Maryland.

[4] Butler, B., Winter, M., Koch, H., Panerai, F., Martin, A., Bailey, S., Stackpoole, M., Danehy, P., and Splinter, S., "Characterization of Candidate Materials for Remote Recession Measurements of Ablative Heat Shield Materials," AIAA SciTech 2016, DOI: 10.2514/6.2016-1516.

[5] Butler, B., Winter, M. W., Stackpoole, "Characterization of Virgin and Charred PICA Seeded for Remote Recession Measurements," AIAA 2017- 3357, 47th AIAA Thermophysics Conference, Denver, CO, 5–9 June 2017.

[6] Trumble, K., Cozmuta, I., Sepka, S., Jenniskens, P., Winter, M., "Post-flight Aerothermal Analysis of the Stardust Sample Return Capsule,' *Journal of Spacecraft and Rockets*, Vol. 47, No. 5, pp. 765-764, Sept.-Oct. 2010.

[7] Winter, M. W., McDaniel, R. D., Chen, Y-K., Liu, Y., Saunders, D., Jenniskens, P., "Radiation Modeling for the Reentry of the Hayabusa Sample Return Capsule," AIAA-2012-1296, *50th AIAA Aerospace Sciences Meeting*, Nashville, Tennessee, 9 - 12 Jan 2012.

[8] Splinter, S. C., Bey, K. S., Gragg, J. G., Brewer, A., "Comparative Measurements of Earth and Martian Entry Environments in the NASA Langley HYMETS Facility," AIAA Paper 2011-1014, *49th AIAA Aerospace Sciences Meeting*, January 4-7, 2011, Orlando, FL, 2011

[9] Johansen, C., Lincoln, D., Bathel, B., Inman, J., Danehy, P., "Simultaneous Laser-Induced Fluorescence of Nitric Oxide and Atomic Oxygen in the Hypersonic Materials Environment Test System Arcjet Facility," *17th International Symposium on Applications of Laser Techniques to Fluid Mechanics*, Lisbon, Portugal, 07-10 July, 2014.